Phase diagram of dense neutral three-flavor quark matter

Stefan B. Rüster,* Igor A. Shovkovy,† and Dirk H. Rischke‡

Institut für Theoretische Physik, J.W. Goethe-Universität,
D-60054 Frankfurt am Main, Germany

(Dated: May 23, 2006)

We study the phase diagram of dense, locally neutral three-flavor quark matter as a function of the strange quark mass, the quark chemical potential, and the temperature, employing a general nine-parameter ansatz for the gap matrix. At zero temperature and small values of the strange quark mass, the ground state of matter corresponds to the color-flavor-locked (CFL) phase. At some critical value of the strange quark mass, this is replaced by the recently proposed gapless CFL (gCFL) phase. We also find several other phases, for instance, a metallic CFL (mCFL) phase, a so-called uSC phase where all colors of up quarks are paired, as well as the standard two-flavor color-superconducting (2SC) phase and the gapless 2SC (g2SC) phase.

I. INTRODUCTION

At sufficiently high densities and sufficiently low temperatures quark matter is a color superconductor [1]. This conclusion follows naturally from arguments similar to those employed in the case of ordinary low-temperature superconductivity in metals and alloys [2]. Of course, the case of quark matter is more complicated because quarks, unlike electrons, come in various flavors (e.g., up, down, and strange) and carry non-Abelian color charges. In the last six years, this phenomenon was studied in detail by various authors [3, 4, 5, 6, 7, 8, 9, 10]. Many different phases were discovered, and recent studies [11, 12, 13, 14, 15, 16] suggest that even more new phases may exist. (For reviews on color superconductivity see, for example, Ref. [17].)

In nature, the most likely place where color superconductivity may occur is the interior of compact stars. Therefore, it is of great importance to study the phases of dense matter under the conditions that are typical for the interior of stars. For example, one should appreciate that matter in the bulk of a star is neutral and β-equilibrated. By making use of rather general arguments, it was suggested in Ref. [21] that such conditions favor the color-flavor-locked (CFL) phase and disfavor the two-flavor superconducting (2SC) phase. In trying to refine the validity of this conclusion, it was recently realized that, depending on the value of the constituent (medium modified) strange quark mass, the ground state of neutral and β-equilibrated dense quark matter may be different from the CFL phase [11, 12, 13, 14, 15, 16]. In particular, the gapless two-flavor color-superconducting (g2SC) phase [11] is likely to be the ground state in the case of a large strange quark mass. On the other hand, in the case of a moderately large strange quark mass, the regular and gapless color-flavor-locked (gCFL) phases [15] are favored. At nonzero temperature, $T \neq 0$, some other phases were proposed as well [16].

In this paper, we study the phase diagram of dense neutral three-flavor quark matter as a function of the strange quark mass at zero and finite temperature. In order to allow for the most general ground state, we employ a nine-parameter ansatz for the gap function. The effects of the strange quark mass are incorporated in our model by a shift of the chemical potential of strange quarks, $\mu_s^i \to \mu_s^i - m_s^2/(2\mu)$ where $i = r, g, b$ is the color index, m_s is the strange quark mass, and μ is the quark chemical potential. This shift reflects the reduction of the Fermi momenta of strange quarks due to their mass. Such an approach is certainly reliable at small values of the strange quark mass. We assume that it is also qualitatively correct at large values of the strange quark mass.

We note that the analysis of this paper is restricted to locally neutral phases only. This automatically excludes, for example, mixed [18] and crystalline [19] phases. Also, in the mean field approximation utilized here, we cannot get any phases with meson condensates [20].

This paper is organized as follows. In Sec. II we present the details of our approach which is based on the Cornwall-Jackiw-Tomboulis (CJT) formalism [22]. There, we also derive the gap equations and the neutrality conditions, and obtain an expression for the pressure. In the next two sections, the gap equations and the neutrality conditions are studied by using numerical methods. The results at zero temperature are presented and discussed in Sec. III. There, the appearance of the CFL and gCFL phases is established in the case of small and moderately large values of the strange quark mass, respectively. The results at nonzero temperature are discussed in Sec. IV. Also, the phase diagram of quark matter in the T–m_s^2/μ plane, as well as in the T–μ plane is presented. Finally, Sec. V concludes this paper with a summary of the results.

Our units are $\hbar = c = k_B = 1$. The metric tensor is $g_{\mu\nu} = \mathrm{diag}\,(1, -1, -1, -1)$. Four-vectors are denoted by capital Latin letters, e.g., $K^\mu = (k^0, \mathbf{k})$ where $\mathbf{k}$ is a three-vector with absolute value $k = |\mathbf{k}|$ and direction $\hat{\mathbf{k}} = \mathbf{k}/k$. We use the imaginary-time formalism, i.e., the

*Electronic address: ruester@th.physik.uni-frankfurt.de
†Electronic address: shovkovy@th.physik.uni-frankfurt.de; on leave of absence from Bogolyubov Institute for Theoretical Physics, 03143, Kiev, Ukraine
‡Electronic address: drischke@th.physik.uni-frankfurt.de

arXiv:hep-ph/0405170 v2 15 Jul 2004

space-time integration is defined as $\int_X = \int_0^{1/T} \mathrm{d}\tau \int_V \mathrm{d}^3\mathbf{x}$, where τ is the Euclidean time coordinate and V the three-volume of the system. Energy-momentum sums are defined as follows: $T/V \sum_K = T \sum_n \int \mathrm{d}^3\mathbf{k}/(2\pi)^3$ where the sum runs over the fermionic Matsubara frequencies $\omega_n = (2n+1)\pi T \equiv ik_0$.

II. MODEL AND FORMALISM

In this paper, we follow closely the approach of Ref. [23] which is based on the CJT formalism [22]. We generalize the model of Ref. [23] in the way that strange quarks may now also participate in forming Cooper pairs. The quark spinor field has the following color-flavor structure:

$$\psi = \begin{pmatrix} \psi_u^r \\ \psi_d^r \\ \psi_s^r \\ \psi_u^g \\ \psi_d^g \\ \psi_s^g \\ \psi_u^b \\ \psi_d^b \\ \psi_s^b \end{pmatrix}. \tag{1}$$

The Dirac conjugate spinor is defined as $\bar{\psi} = \psi^\dagger \gamma_0$. In the treatment of superconducting systems it is advantageous to double the fermionic degrees of freedom by introducing the so-called Nambu-Gorkov spinors

$$\bar{\Psi} = \left(\bar{\psi}, \bar{\psi}_C \right), \qquad \Psi = \begin{pmatrix} \psi \\ \psi_C \end{pmatrix}, \tag{2}$$

where $\psi_C = C\bar{\psi}^T$ is the charge-conjugate spinor, and C is the charge-conjugation matrix.

In this paper, as in Ref. [23], we shall approximate the gluon-exchange interaction between the quarks by a point-like current-current interaction. Physically, this is equivalent to a model with heavy, non-dynamical gluons. In many ways, such an approximation is analogous to the nonrenormalizable Fermi theory of weak interactions that was used before the SU(2)×U(1) gauge theory of electroweak forces was developed [24]. Also, in the mean-field approximation that we use below, our treatment will be similar to that in Refs. [3, 4, 11, 12, 14, 15, 25, 26, 27] which are based on Nambu–Jona-Lasinio (NJL) [28] type models.

In the approximation with a point-like interaction, the CJT effective action simplifies. It has the following general form:

$$\Gamma\left[\mathcal{S}\right] = \frac{1}{2}\mathrm{Tr}\ln\mathcal{S}^{-1} + \frac{1}{2}\mathrm{Tr}\left(S_0^{-1}\mathcal{S} - 1\right) + \Gamma_2\left[\mathcal{S}\right]. \tag{3}$$

Here the traces run over space-time, Nambu-Gorkov, color, flavor, and Dirac indices. The factor $1/2$ in front of the fermionic one-loop terms compensates the doubling of the degrees of freedom in the Nambu-Gorkov basis.

In the above effective action, $\mathcal{S}$ denotes the full quark propagator.

In order to understand the structure of the full quark propagator $\mathcal{S}$, let us first discuss the structure of the free quark propagator S_0 in the Nambu-Gorkov basis. The inverse, S_0^{-1}, is given by the following matrix:

$$S_0^{-1} = \begin{pmatrix} [G_0^+]^{-1} & 0 \\ 0 & [G_0^-]^{-1} \end{pmatrix}, \tag{4}$$

where

$$[G_0^\pm]^{-1} = \gamma^\mu K_\mu \pm \hat{\mu}\gamma_0 \tag{5}$$

are the inverse Dirac propagators for massless quarks and charge-conjugate quarks, respectively. At sufficiently large quark chemical potential, there is no need to take into account the small masses of the light up- and down-quarks. It is easy to understand that the dynamical effect of such masses around the quark Fermi surfaces is negligible. Of course, the situation with the strange quark is different because its mass is not very small as compared to μ. It appears, however, that the most important effect of a nonzero strange quark mass is a shift of the strange quark chemical potential due to the reduction of the Fermi momentum, $\mu_s^i \to \mu_s^i - m_s^2/(2\mu)$. (Strictly speaking, it is μ_s^i rather than μ that should appear in the denominator. Quantitatively, however, this does not make a big difference.) For simplicity, this is the only mass effect that we include in our analysis below. Note that nonzero quark masses were properly accounted for in Refs. [26, 27, 29].

The quark chemical potential matrix $\hat{\mu}$ in color-flavor space is defined as

$$\hat{\mu} = \mathrm{diag}\left(\mu_u^r, \mu_d^r, \mu_s^r, \mu_u^g, \mu_d^g, \mu_s^g, \mu_u^b, \mu_d^b, \mu_s^b\right). \tag{6}$$

In realistic systems, such as bulk matter inside a star, some of the μ_f^i should be related. This is because, in chemical equilibrium, one can introduce only as many independent chemical potentials as there are different conserved charges in the system. In quark matter, the chemical potentials μ_f^i can be defined in terms of the quark chemical potential μ ($\mu \equiv \mu_B/3$, where μ_B is the baryon chemical potential), the chemical potential μ_Q for the electrical charge, and the two chemical potentials, μ_3 and μ_8, for color charge,

$$\mu_f^i = \mu + \mu_Q Q_f + \mu_3 T_3^i + \mu_8 T_8^i. \tag{7}$$

Thus, there are only four out of nine chemical potentials in Eq. (6) that are independent in the case of dense three-flavor quark matter in chemical equilibrium. In (locally) neutral matter, as we shall see below, only one of them will remain independent.

In the framework of the CJT formalism, the thermodynamic potential of quark matter is proportional to the CJT effective action at its stationary point, determined by the solution of the following equation:

$$\frac{\delta\Gamma}{\delta\mathcal{S}} = 0. \tag{8}$$

This is nothing but the Dyson-Schwinger equation for the quark propagator,

$$\mathcal{S}^{-1} = S_0^{-1} + \Sigma \,, \tag{9}$$

where

$$\Sigma \equiv 2\frac{\delta\Gamma_2\left[\mathcal{S}\right]}{\delta\mathcal{S}} \tag{10}$$

is the quark self-energy. The functional Γ_2 is the sum of all two-particle irreducible (2PI) diagrams. Unfortunately, it is impossible to evaluate all 2PI diagrams exactly. Nevertheless, the advantage of the CJT effective action (3) is that a truncation of the sum Γ_2 at a finite number of terms still provides a well-defined many-body approximation. In this study, we only include the sunset-type diagram shown in Fig. 1 of Ref. [23], which becomes a double-bubble diagram in the case of a local, instantaneous interaction. It is easy to check that this leads to the following expression for the self-energy:

$$\Sigma\left(K\right) = -g^2\frac{T}{V}\sum_Q \Gamma_a^\mu \mathcal{S}\left(Q\right)\Gamma_b^\nu D_{\mu\nu}^{ab} \,. \tag{11}$$

Local, instantaneous gluon exchange is parametrized by a propagator of the form

$$D_{\mu\nu}^{ab} \equiv -\delta^{ab}\frac{g_{\mu\nu}}{\Lambda^2}. \tag{12}$$

In Eq. (11), we introduced the Nambu-Gorkov vertex,

$$\Gamma_a^\mu = \begin{pmatrix} \gamma^\mu T_a & 0 \\ 0 & -\gamma^\mu T_a^T \end{pmatrix}. \tag{13}$$

Equation (11) is a self-consistency equation for Σ, commonly called the "gap equation".

In color-superconducting systems, the quark self-energy has the form

$$\Sigma = \begin{pmatrix} 0 & \Phi^- \\ \Phi^+ & 0 \end{pmatrix}. \tag{14}$$

The regular (diagonal) part of the self-energy is neglected here. While it plays an important role in the dynamics of chiral symmetry breaking, it is essentially irrelevant for color superconductivity in dense quark matter. (The effect of the diagonal part of the self-energy was studied, for example, in Ref. [6].) The off-diagonal elements Φ^- and Φ^+ in Eq. (14) are matrices in Dirac, color and flavor space. They are related by the requirement that the action is real, $\Phi^- \equiv \gamma^0\left(\Phi^+\right)^\dagger\gamma^0$.

With Eq. (14) one may invert Eq. (9) to obtain the full quark propagator,

$$\mathcal{S} = \begin{pmatrix} G^+ & \Xi^- \\ \Xi^+ & G^- \end{pmatrix} \,, \tag{15}$$

where the diagonal and off-diagonal elements are

$$G^\pm = \left\{[G_0^\pm]^{-1} - \Phi^\mp G_0^\mp \Phi^\pm\right\}^{-1} \tag{16}$$

and

$$\Xi^\pm = -G_0^\mp\Phi^\pm G^\pm, \tag{17}$$

respectively.

In the following, we use the notation Γ^* for the CJT effective action evaluated at the stationary point. In the approximation used here, it takes the following form:

$$\Gamma^* = \frac{1}{2}\mathrm{Tr}\ln\mathcal{S}^{-1} - \frac{1}{4}\mathrm{Tr}\left(\Sigma\mathcal{S}\right) \,, \tag{18}$$

In this paper, we utilize the following nine-parameter ansatz for the gap matrix:

$$\Phi^\pm = \begin{pmatrix} [\Delta_{uu}^{rr}]^\pm & 0 & 0 & 0 & [\Delta_{ud}^{rg}]^\pm & 0 & 0 & 0 & [\Delta_{us}^{rb}]^\pm \\ 0 & 0 & 0 & [\Delta_{du}^{rg}]^\pm & 0 & 0 & 0 & 0 & 0 \\ 0 & 0 & 0 & 0 & 0 & 0 & [\Delta_{su}^{rb}]^\pm & 0 & 0 \\ 0 & [\Delta_{du}^{rg}]^\pm & 0 & 0 & 0 & 0 & 0 & 0 & 0 \\ [\Delta_{ud}^{rg}]^\pm & 0 & 0 & 0 & [\Delta_{dd}^{gg}]^\pm & 0 & 0 & 0 & [\Delta_{ds}^{gb}]^\pm \\ 0 & 0 & 0 & 0 & 0 & 0 & 0 & [\Delta_{sd}^{gb}]^\pm & 0 \\ 0 & 0 & [\Delta_{su}^{rb}]^\pm & 0 & 0 & 0 & 0 & 0 & 0 \\ 0 & 0 & 0 & 0 & 0 & [\Delta_{sd}^{gb}]^\pm & 0 & 0 & 0 \\ [\Delta_{us}^{rb}]^\pm & 0 & 0 & 0 & [\Delta_{ds}^{gb}]^\pm & 0 & 0 & 0 & [\Delta_{ss}^{bb}]^\pm \end{pmatrix}. \tag{19}$$

The explicit Dirac structure of the matrix elements is

$$\left[\Delta_{ff'}^{ii'}\right]^+\left(K\right) = \sum_{c,e=\pm} \phi_{cff'}^{eii'}\left(K\right)\mathcal{P}_c^e(\mathbf{k}) \,, \tag{20a}$$

$$\left[\Delta_{ff'}^{ii'}\right]^-\left(K\right) = \sum_{c,e=\pm} \phi_{cff'}^{eii'}\left(K\right)\mathcal{P}_{-c}^{-e}(\mathbf{k}) \,. \tag{20b}$$

In this representation, $\phi_{cff'}^{eii'}$ are real-valued gap para-

meters, while

$$\mathcal{P}_c^e(\mathbf{k}) = \tfrac{1}{4} \left(1 + c\gamma_5\right)(1 + e\gamma_0\boldsymbol{\gamma}\cdot\hat{\mathbf{k}}) \qquad (21)$$

are the energy-chirality projectors.

In order to calculate the first part of the effective action in Eq. (18), we transform the inverse quark propagator (9) into a block-diagonal form which is schematically shown in Fig. 1. This is easily achieved by changing the order of rows and columns in color, flavor, and Nambu-Gorkov space. The energy-chirality projectors simplify the calculation of the Dirac traces. After performing these traces, we use the matrix relation $\mathrm{Tr}\ln A = \sum_K \ln\left(\det A\right)$ to calculate the one-loop contribution of the quarks to Γ^*.
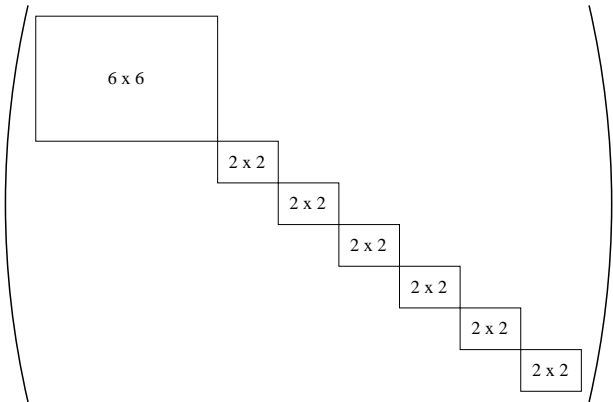
FIG. 1: The block-diagonal structure of the inverse quark propagator in color-flavor and Nambu-Gorkov space.

We use the Gauss elimination procedure to reduce the 6×6-block to a 3×3-block and all the 2×2-blocks to 1×1-blocks in color-flavor space. The determinant of the 3×3-block is computed analytically by using, for example, Mathematica or Maple.

The most complicated expression arises from the determinant of the 3×3-block. Schematically, it has the following form:

$$\det\left(3 \times 3\right)_e = k_0^6 + b k_0^4 + c k_0^2 + d. \qquad (22)$$

Here, the coefficients b, c, and d are rather complicated functions of the quark momentum k, three che-

mical potentials (μ_u^r, μ_d^g, and μ_s^b) and six gap parameters (ϕ_{uu}^{rr}, ϕ_{ud}^{rg}, ϕ_{us}^{rb}, ϕ_{dd}^{gg}, ϕ_{ds}^{gb}, and ϕ_{ss}^{bb}). This determinant can always be factorized as follows: $\det\left(3 \times 3\right)_e \equiv [k_0^2 - (\tilde{\epsilon}_1^e)^2][k_0^2 - (\tilde{\epsilon}_2^e)^2][k_0^2 - (\tilde{\epsilon}_3^e)^2]$. As is clear, the functions $\tilde{\epsilon}_1^e$, $\tilde{\epsilon}_2^e$ and $\tilde{\epsilon}_3^e$ determine the dispersion relations of the three quasiparticles described by the 3×3-block of the quark propagator. In order to get their explicit expressions, one solves the cubic equation $\det\left(3 \times 3\right)_e = 0$ for $\xi = k_0^2$. By making use of Cardano's formula, the solutions can be presented in an analytical form that we use later in the numerical calculations. Because of their very complicated nature we refrain from presenting them explicitly.

The dispersion relations of the quasiparticles that correspond to the 1×1-blocks are easy to derive. They are given in terms of the same function, $\epsilon_{\mathbf{k}}^e(\mu,\phi) = [(k - e\mu)^2 + |\phi|^2]^{1/2}$, that also appears in the 2SC phase.

Once the quasiparticle dispersion relations are established, the calculation of the first term in the CJT action, i.e., $\sum_K \ln\left(\det\mathcal{S}^{-1}\right) \equiv \sum_j \sum_K \ln\left[(\omega_n + i\mu_j)^2 + \epsilon_j^2\right]$, reduces to a sum of several standard contributions of the following type [30]:

$$\sum_K \ln\left(\frac{(\omega_n + i\mu_j)^2 + \epsilon_j^2}{T^2}\right) = V \int \frac{p^2 dp}{2\pi^2}\left[\frac{\epsilon_j}{T}\right.$$
$$\left. + \ln\left(1 + \mathrm{e}^{-(\epsilon_j - \mu_j)/T}\right) + \ln\left(1 + \mathrm{e}^{-(\epsilon_j + \mu_j)/T}\right)\right]. \quad (23)$$

In order to simplify the second term in the effective potential in Eq. (18), we use the gap equation (11). Then, we arrive at the following simple result:

$$-\frac{1}{4}\mathrm{Tr}\left(\Sigma S\right) = \frac{3}{4}\frac{\Lambda^2}{g^2}\frac{V}{T}\,\mathrm{Tr}\left[\hat{\Phi}\left(\hat{\Phi} + 3\sum_a T_a^T\hat{\Phi}T_a\right)\right], \quad (24)$$

where the new notation $\hat{\Phi}$ was introduced to represent only the color-flavor part of the gap matrix Φ^+, given in Eq. (19). In this connection, it should be noted that the gap parameters $\phi_{cff'}^{eii'}$ are independent of the chirality and energy projections. This is a consequence of the gap equation (11).

Finally, by combining all contributions to Eq. (18), we derive the result for the pressure $p \equiv \frac{T}{V}\Gamma^*$,

$$p = \frac{T}{\pi^2} \sum_l \int_0^\infty \mathrm{d}k\, k^2 \left\{ \ln\left[1 + \exp\left(-\frac{E_l - \mu_l}{T}\right)\right] + \ln\left[1 + \exp\left(-\frac{E_l + \mu_l}{T}\right)\right] \right\}$$

$$+ \frac{3}{4}\frac{\Lambda^2}{g^2} \sum_{i=1}^3 \left(\phi_i^2 + \varphi_i^2 + 6\phi_i\varphi_i + 2\sigma_i^2\right) + \frac{1}{2\pi^2} \sum_{i=1}^3 \sum_{e=\pm} \int_0^\kappa \mathrm{d}k\, k^2 \left\{ \tilde{\epsilon}_i^e - k + 2T \ln\left[1 + \exp\left(-\frac{\tilde{\epsilon}_i^e}{T}\right)\right] \right\}$$

$$+ \frac{1}{\pi^2} \sum_{i=1}^3 \sum_{e=\pm} \int_0^\kappa \mathrm{d}k\, k^2 \left\{ \epsilon_{\mathbf{k}}^e\left(\bar{\mu}_i, \phi_i\right) - k + T \ln\left[1 + \exp\left(-\frac{\epsilon_{\mathbf{k}}^e\left(\bar{\mu}_i, \phi_i\right) + \delta\mu_i}{T}\right)\right] \right.$$

$$\left. + T \ln\left[1 + \exp\left(-\frac{\epsilon_{\mathbf{k}}^e\left(\bar{\mu}_i, \phi_i\right) - \delta\mu_i}{T}\right)\right] \right\} . \tag{25}$$

The first term in this expression is the contribution of leptons (i.e., $l = e^-, \mu^-$). In principle, the contribution of neutrinos should be added as well. In this paper, however, their contribution is neglected. This is a good approximation for compact stars after deleptonization. The dispersion relations of the leptons are given by $E_l = \sqrt{k^2 + m_l^2}$ with $m_{e^-} \approx 0.511$ MeV and $m_{\mu^-} \approx 105.66$ MeV. Note that the vacuum contribution was subtracted in Eq. (25), in order to improve the convergence of the momentum integrals. In various applications, a bag constant could be added if necessary. In Eq. (25), ϕ_i are the three independent gap parameters that appear in the 2×2-blocks in Fig. 1, while φ_i and σ_i appear in the 6×6-block. They are defined by

$$\phi_1 \equiv \phi_{sd}^{gb}, \qquad \varphi_1 \equiv \phi_{ds}^{gb}, \quad \text{and} \quad \sigma_1 \equiv \phi_{uu}^{rr}, \tag{26a}$$

$$\phi_2 \equiv \phi_{su}^{rb}, \qquad \varphi_2 \equiv \phi_{us}^{rb}, \quad \text{and} \quad \sigma_2 \equiv \phi_{dd}^{gg}, \tag{26b}$$

$$\phi_3 \equiv \phi_{du}^{rg}, \qquad \varphi_3 \equiv \phi_{ud}^{rg}, \quad \text{and} \quad \sigma_3 \equiv \phi_{ss}^{bb}. \tag{26c}$$

In accordance with the fact that the gap parameters are independent of the energy and chirality, the corresponding indices were dropped. Similarly, $\bar{\mu}_i$ and $\delta\mu_i$ $(i = 1, 2, 3)$ are the average values and the differences of various pairs of chemical potentials that come from the three different 2×2-blocks,

$$\bar{\mu}_1 \equiv \frac{1}{2}(\mu_s^g + \mu_d^b), \quad \text{and} \quad \delta\mu_1 \equiv \frac{1}{2}(\mu_s^g - \mu_d^b), \tag{27a}$$

$$\bar{\mu}_2 \equiv \frac{1}{2}(\mu_s^r + \mu_u^b), \quad \text{and} \quad \delta\mu_2 \equiv \frac{1}{2}(\mu_s^r - \mu_u^b), \tag{27b}$$

$$\bar{\mu}_3 \equiv \frac{1}{2}(\mu_d^r + \mu_u^g), \quad \text{and} \quad \delta\mu_3 \equiv \frac{1}{2}(\mu_d^r - \mu_u^g). \tag{27c}$$

In order to render the integrals in the expression for the pressure finite, we introduced a three-momentum cutoff κ. In QCD with dynamical gluons, of course, such a cutoff would not be necessary. Here, however, we use a model with a local current-current interaction which is nonrenormalizable.

In the case of the ansatz (19) for the gap function, there are nine coupled gap equations (corresponding to the total number of gap parameters) that follow from Eq. (11). The explicit form of these equations is very complicated

and not very informative by itself. Because of this, they will not be displayed here. In the next two sections, we solve these gap equations by numerical methods.

As was mentioned in the Introduction, matter in the bulk of a compact star should satisfy the conditions of charge neutrality and β-equilibrium. The latter is automatically satisfied after choosing the chemical potentials as in Eq. (7). The neutrality conditions read

$$n_Q \equiv \frac{\partial p}{\partial \mu_Q} = 0 , \tag{28a}$$

$$n_3 \equiv \frac{\partial p}{\partial \mu_3} = 0 , \tag{28b}$$

$$n_8 \equiv \frac{\partial p}{\partial \mu_8} = 0 . \tag{28c}$$

After solving these equations, one is left with only one chemical potential (out of four) that remains independent. It is most convenient to keep the quark chemical potential μ as a free parameter, and determine μ_Q, μ_3 and μ_8 from Eqs. (28). This is done numerically.

III. RESULTS AT ZERO TEMPERATURE

In this section we focus on three-flavor quark matter at zero temperature. It is clear that, for small and moderate values of the strange quark mass, the ground state of neutral quark matter should correspond to either the regular (gapped) CFL phase [4] or the gapless CFL phase [15]. At very large strange quark mass and/or relatively weak coupling, the ground state can also be either a regular (gapped) or gapless 2SC color superconductor [11].

Before proceeding to the results, let us specify the parameters of the model. The strength of the diquark coupling and the value of the cutoff in the momentum integrals are fixed as follows:

$$g^2/\Lambda^2 = 45.1467 \text{ GeV}^{-2} , \tag{29a}$$

$$\kappa = 0.6533 \text{ GeV} . \tag{29b}$$

In order to see how the phase structure of neutral three-flavor quark matter changes with the mass of the strange

quark m_s, we solve a coupled set of twelve equations, i.e., nine gap equations and three neutrality conditions, given in Eq. (28), for various values of m_s, keeping the quark chemical potential fixed. In this calculation we take $\mu = 500$ MeV. The results for the absolute values of the gap parameters and the chemical potentials μ_Q, μ_3, and μ_8 are shown in Figs. 2 and 3, respectively. Note that, strictly speaking, the gap parameters do not coincide with the actual values of the gaps in the quasiparticle spectra. In the case of the CFL phase, for example, there is a degenerate octet of quasiparticles with a gap $\phi_{\text{octet}} = |\phi_1|$ and a singlet state with a gap $\phi_{\text{singlet}} = 3\varphi_1 - |\phi_1|$. In the CFL phase, $\phi_1 = \phi_2 = \phi_3 < 0$, $\varphi_1 = \varphi_2 = \varphi_3 > 0$, and $\sigma_1 = \sigma_2 = \sigma_3 > 0$. Also, in the CFL phase, the following relation between the gap parameters is satisfied: $\sigma_i = \varphi_i - |\phi_i| \equiv 2\phi_{(6,6)}$, $i = 1, 2, 3$, where $\phi_{(6,6)}$ is the sextet-sextet gap in the notation of Ref. [7].

The results in Figs. 2 and 3 extend the results of Ref. [15] by considering a more general ansatz for the gap matrix that takes into account, in particular, the pairing in the symmetric sextet-sextet channel. The effect of including pairing in the symmetric channel is a splitting between the pairs of gaps $(|\phi_1|, \varphi_1)$, $(|\phi_2|, \varphi_2)$ and $(|\phi_3|, \varphi_3)$ that is also reflected in the change of the quasiparticle spectra. Of course, in agreement with the general arguments of Refs. [4, 7], the symmetric sextet-sextet gaps are rather small, see Fig. 2 (c). This, in turn, explains the fact why the splittings between the above mentioned pairs of gap parameters are not very large [compare the results in Figs. 2 (a) and (b)].

In this study, we confirm that the phase transition from the CFL phase to the gCFL phase happens at a critical value of the parameter m_s^2/μ that is in good agreement with the simple estimate of Ref. [15],

$$\frac{m_s^2}{\mu} \simeq 2\Delta \sim 190 \text{ MeV}. \qquad (30)$$

The qualitative results for the chemical potentials μ_Q, μ_3, and μ_8 in Fig. 3 are in agreement with the corresponding results obtained in Ref. [15] as well. In the CFL phase, in our notation the color chemical potential μ_8 fulfils the identity $\mu_8 = -m_s^2/(\sqrt{3}\mu)$. In addition, while the CFL phase requires no electrons to remain neutral, the pairing in the gCFL phase is distorted and a finite density of electrons appears. This is seen directly from the dependence of the electrical chemical potential μ_Q in Fig. 3, which becomes nonzero only in the gCFL phase. This observation led the authors of Ref. [15] to the conclusion that the phase transition between the CFL and gCFL phase is an insulator-metal phase transition, and that the value of the electron density is a convenient order parameter in the description of such a transition. In fact, one could also choose one of the differences between number densities of mutually paired quarks as an alternative choice for the order parameter [11]. In either case, there does not seem to exist any continuous symmetry that is associated with such an order parameter. To complete the discussion

of the chemical potentials, we add that the other color chemical potential, μ_3, is zero only in the CFL phase at $T = 0$.

The effects of a nonzero strange quark mass on the phase structure of neutral strange quark matter could be viewed from a different standpoint that, in application to stars, may look more natural. This is the case where the dependence on the quark chemical potential is studied at a fixed value of m_s. The corresponding numerical results are shown in Fig. 4. (Note once again that ϕ_i with $i = 1, 2, 3$ have negative values, and we always plot their absolute values.) In this particular calculation we choose $m_s = 300$ MeV.

At large values of the quark chemical potential [$\mu \gtrsim m_s^2/(2\Delta) \sim 475$ MeV which is similar to the small strange quark mass limit considered before], the ground state of quark matter is the CFL phase. At smaller values of the chemical potential, the ground state of dense matter is the gCFL phase. In this case, there are nine gap parameters all of which are different from each other. One could also check that the density of quarks that pair are not equal in the gCFL phase. This can be seen from Fig. 5 where all nine quark number densities are plotted for the same value of the strange quark mass, $m_s = 300$ MeV. Only $n_d^r = n_u^g$ and $n_s^r \approx n_u^b$, all other quark number densities are different from each other. This agrees with the general criterion of the appearance of gapless phases at $T = 0$ that was proposed in Ref. [11] in the case of two-flavor quark matter. In the ordinary CFL phase, in contrast, one finds that $n_u^r = n_d^g = n_s^b$, and $n_d^r = n_s^r = n_u^g = n_s^g = n_u^b = n_d^b$.

In order to see that the gCFL phase indeed describes a gapless superconductor, it is necessary to show that the dispersion relations of quasiparticles contain gapless excitations. In Fig. 6, the dispersion relations of all nine quasiparticles are plotted. The dispersion relations for the corresponding anti-particles are not shown. The dispersion relations that result from the 6×6 color-flavor block of the quark propagator are labelled by $\tilde{\epsilon}_i$ in Fig. 6 (see the discussion and Fig. 1 in Sec. II). The remaining dispersion relations correspond to quasiparticles that are described by the 2×2-blocks of the quark propagator, given by $k_0 = \epsilon_{\mathbf{k}}^e(\bar{\mu}_i, \phi_i) \pm \delta\mu_i$. Qualitatively, these are the same as the dispersion relations that appear in the 2SC/g2SC phase in Ref. [11]. This is not a coincidence because the corresponding 2×2 color-flavor blocks of the propagator have the same structure as in the case of the 2SC/g2SC phase.

From Fig. 6 we see that there is indeed a gapless mode in the "green-strange–blue-down" sector. This is the same that was found in Ref. [15]. Note also that, in agreement with Ref. [15], the "red-strange–blue-up" quasiparticle has a dispersion relation that is nearly quadratic, $k_{0su}^{rb} \simeq |k - k^*|^2$ with $k^* \approx 400$ MeV for a given choice of parameters, see Fig. 6 (c). The nearly quadratic dispersion relation resembles the situation at the transition between the 2SC phase, where $n_u^r = n_d^g$, and the gapless 2SC phase, where n_u^r and n_d^g are diffe-

rent. This explains the approximate equality $n_s^r \approx n_u^b$ mentioned above.

IV. RESULTS AT NONZERO TEMPERATURE

In this section, we present the results for the phase structure of dense neutral three-flavor quark matter in the plane of temperature and m_s^2/μ, as well as in the plane of temperature and quark chemical potential.

Let us start with the discussion of the temperature dependence of the gap parameters in the two qualitatively different cases of small and large values of the strange quark mass. As we saw in the previous section, the zero-temperature properties of neutral quark matter were very different in these two limits.

The results for the temperature dependence of the gap parameters are shown in Figs. 7, 8 and 9 for two different values of the strange quark mass that represent the two qualitatively different regimes. In the case of a small strange quark mass (i.e., the case of $m_s^2/\mu = 80$ MeV which is shown in Figs. 7 and 8), the zero-temperature limit corresponds to the CFL phase. This is seen from the fact that the three different gaps shown in every panel of Fig. 7 merge as $T \to 0$. At nonzero temperature, on the other hand, the gap parameters are not the same. This suggests that, similar to the zero-temperature case of Figs. 2 and 4, a phase transition to the gCFL phase happens at some nonzero temperature. However, we shall show below that there is no phase transition between the CFL and gCFL phases at *any* nonzero temperature. Instead, there is an insulator-metal crossover transition between the CFL phase and a so-called *metallic* CFL (mCFL) phase. At this point, all quasiparticles are still gapped. At some higher temperature, the mCFL phase is replaced by the gCFL phase.

If the temperature is increased even further, there are three consecutive phase transitions. These correspond to the three phase transitions predicted in Ref. [16] in the limit of a small strange quark mass. In order to resolve these, we show a close-up of the near-critical region of Fig. 7 in Fig. 8. The three transitions that we observe are the following: (i) transition from the gCFL phase to the so-called uSC phase; (ii) transition from the uSC phase to the 2SC phase; (ii) transition from the 2SC phase to the normal quark phase. Here, the notation uSC (dSC) stands for superconductivity in which all three colors of up (down) quark flavor participate in diquark pairing [16]. Our results differ from those of Ref. [16] in that the dSC phase is replaced by the uSC phase. The reason is that, in our case, the first gaps which vanish with increasing temperature are ϕ_1 and φ_1, see Fig. 8, while in their case Δ_2 (corresponding to our ϕ_2 and φ_2) disappears first. Although we use the same terms for the phases that were introduced in Ref. [16], we distinguish between the gapped phases (e.g., CFL and mCFL phase) and the gapless phases (e.g., gCFL). Also, in order to reflect the physical properties of the mCFL phase, we

suggest to use the term *metallic* CFL, instead of *modified* CFL as in Ref. [16]. (Note that, in that work, the mCFL phase also encompasses the gCFL phase.)

In the case of a large strange quark mass (i.e., the case of $m_s^2/\mu = 320$ MeV shown in Fig. 9), the zero-temperature limit corresponds to the gCFL phase. By looking at the corresponding temperature dependence of the gap parameters, we see that this case is a natural generalization of the previous limit of a small strange quark mass. There are also three consecutive phase transitions. It is noticeable, however, that the separation between the different transitions becomes much wider at large m_s.

We now take a closer look at the transition between the CFL, the mCFL, and the gCFL phase. Let us recall that, at zero temperature, there was no symmetry connected with the order parameter, i.e., the number density of electrons, that is associated with the CFL $\to$ gCFL phase transition. At nonzero temperature, the electron density is not strictly zero in the CFL phase as soon as $m_s \neq 0$. Indeed, the arguments of Ref. [31] regarding the enforced neutrality of the CFL phase do not apply at $T \neq 0$. This leads us to the conclusion that the insulator-metal transition between the CFL and the mCFL phase is just a smooth crossover at $T \neq 0$. Of course, in principle, we can never exclude the existence of a first-order phase transition. Our numerical analysis, however, reveals a crossover. The transition can only be identified by a rapid increase of the electron density in a relatively narrow window of temperatures, see Fig. 10 (a). The location of the maximum of the corresponding "susceptibility" (i.e., dn_Q/dT) is then associated with the transition point.

The transition between the mCFL and the gCFL phase corresponds to the appearance of gapless quasiparticle modes in the spectrum. We do not yet know whether this transition is associated with any physical susceptibility. There is no way of telling from the temperature dependences in Figs. 7, 8 and 9, whether the corresponding CFL and/or 2SC phases are gapless or not. This additional piece of information can only be extracted from the behavior of the quasiparticle spectra. We also investigated them, but we do not show them explicitly.

Our results for the phase structure of dense neutral three-flavor quark matter are summarized in Fig. 11. We show the phase diagram in the T–m_s^2/μ plane at a fixed value of the quark chemical potential, $\mu = 500$ MeV, and in the T–μ plane at a fixed value of the strange quark mass, $m_s = 250$ MeV. The three solid lines denote the three phase transitions discussed above. The two dashed lines mark the appearance of gapless modes in the mCFL and 2SC phases. We could term these as the mCFL $\to$ gCFL and 2SC $\to$ g2SC crossover transitions. In addition, as we mentioned above, there is also an insulator-metal type transition between the CFL and mCFL phase. This is marked by the dotted lines in Fig. 11.

V. CONCLUSIONS

In this paper, we studied neutral three-flavor quark matter at large baryon densities. We obtained a very rich phase structure by varying the strange quark mass, the quark chemical potential, and the temperature.

At $T = 0$, there are two main possibilities for the strange quark matter ground state: the CFL and gCFL phases. These findings confirm the results of Ref. [15] concerning the existence of the gapless CFL phase, the estimate of the critical value of the strange quark mass m_s, and the dependence of the chemical potentials on m_s. We also confirm that it is the color neutrality condition, controlled by the color chemical potential μ_8 which drives the transition from the CFL to the gCFL phase [15]. This is in contrast to gapless 2SC superconductivity which results from electrical neutrality [11].

Because we use a nine-parameter ansatz for the gap function, the results of this paper are more general than those of Ref. [15]. For example, we were able to explicitly study the effects of the symmetric pairing channel, described by the sextet-sextet gap parameters, that were neglected in Ref. [15]. As one might have expected, these latter modify the quasiparticle dispersion relations only slightly. This check was important, however, to see that the zero-temperature phase transition from the CFL phase to the gapless CFL phase, which is not associated with any symmetry, is robust against such a deformation of the quark system.

In this paper, we also studied the temperature dependence of the gap parameters and the quasiparticle spectra. In particular, this study revealed that there exist several different phases of neutral three-flavor quark matter that have been predicted in the framework of the Ginzburg-Landau-type effective theory in Ref. [16]. Our results extend the near-critical behavior discussed in Ref. [16] to all temperatures. Also, we show how this behavior evolves with changing the value of the strange quark mass. The only real qualitative difference between our results and the results of Ref. [16] is that, instead of the dSC phase, we find the uSC phase in the phase diagram.

The main result of our paper is the complete phase diagram of neutral three-flavor quark matter in the T–m_s^2/μ and T–μ plane, shown in Fig. 11. In this figure, all symmetry related phase transitions are denoted by solid lines. (The symmetries of all phases appearing in this figure were discussed in Ref. [16].) In the mean-field approximation used here, all of these transitions are second-order phase transitions. After taking into account various types of fluctuations, the nature of some of them may change [32]. A detailed study of this issue is, however, outside the scope of this paper. The dashed lines in Fig. 11 separate the mCFL and regular 2SC phases from the gapless CFL and gapless 2SC phases. These cannot be real phase transitions, but are at most smooth crossovers. At $T = 0$, there is an insulator-metal phase transition between the CFL and the gCFL phase [15]. At nonzero temperature, there exists a similar insulator-metal type transition between the CFL and the mCFL phase, given by the dotted lines in Fig. 11.

[1] B. C. Barrois, Nucl. Phys. B **129**, 390 (1977); S. C. Frautschi, in "Hadronic matter at extreme energy density", edited by N. Cabibbo and L. Sertorio (Plenum Press, 1980); D. Bailin and A. Love, Phys. Rep. **107**, 325 (1984).

[2] J. R. Schrieffer, *Theory of Superconductivity* (Benjamin, New York, 1964).

[3] M. Alford, K. Rajagopal, and F. Wilczek, Phys. Lett. B **422**, 247 (1998); R. Rapp, T. Schäfer, E. V. Shuryak, and M. Velkovsky, Phys. Rev. Lett. **81**, 53 (1998).

[4] M. G. Alford, K. Rajagopal, and F. Wilczek, Nucl. Phys. **B537**, 443 (1999).

[5] D. T. Son, Phys. Rev. D **59**, 094019 (1999); T. Schäfer and F. Wilczek, Phys. Rev. D **60**, 114033 (1999); D. K. Hong, V. A. Miransky, I. A. Shovkovy, and L. C. R. Wijewardhana, Phys. Rev. D **61**, 056001 (2000); R.D. Pisarski and D.H. Rischke, Phys. Rev. D **61**, 051501 (2000); Phys. Rev. D **61**, 074017 (2000); S. D. H. Hsu and M. Schwetz, Nucl. Phys. **B572**, 211 (2000).

[6] W. E. Brown, J. T. Liu, and H.-c. Ren, Phys. Rev. D **61**, 114012 (2000); Q. Wang and D. H. Rischke, Phys. Rev. D **65**, 054005 (2002).

[7] I. A. Shovkovy and L. C. R. Wijewardhana, Phys. Lett. B **470**, 189 (1999); T. Schäfer, Nucl. Phys. **B575**, 269 (2000).

[8] M. G. Alford, J. A. Bowers, and K. Rajagopal, Phys. Rev. D **63**, 074016 (2001); J. A. Bowers, J. Kundu, K. Rajagopal, and E. Shuster, Phys. Rev. D **64**, 014024 (2001); R. Casalbuoni, R. Gatto, M. Mannarelli, and G. Nardulli, Phys. Rev. D **66**, 014006 (2002); I. Giannakis, J. T. Liu, and H.-c. Ren, Phys. Rev. D **66**, 031501 (2002); J. A. Bowers and K. Rajagopal, Phys. Rev. D **66**, 065002 (2002).

[9] T. Schäfer, Phys. Rev. D **62**, 094007 (2000); M. G. Alford, J. A. Bowers, J. M. Cheyne, and G. A. Cowan, Phys. Rev. D **67**, 054018 (2003); M. Buballa, J. Hošek, and M. Oertel, Phys. Rev. Lett. **90**, 182002 (2003).

[10] A. Schmitt, Q. Wang, and D. H. Rischke, Phys. Rev. Lett. **91**, 242301 (2003); nucl-th/0311006.

[11] I. Shovkovy and M. Huang, Phys. Lett. B **564**, 205

(2003); M. Huang and I. Shovkovy, Nucl. Phys. A **729**, 835 (2003).

[12] E. Gubankova, W. V. Liu, and F. Wilczek, Phys. Rev. Lett. **91**, 032001 (2003).

[13] A. Mishra and H. Mishra, Phys. Rev. D **69**, 014014 (2004).

[14] J. F. Liao and P. F. Zhuang, Phys. Rev. D **68**, 114016 (2003).

[15] M. Alford, C. Kouvaris, and K. Rajagopal, hep-ph/0311286.

[16] K. Iida, T. Matsuura, M. Tachibana, and T. Hatsuda, hep-ph/0312363.

[17] K. Rajagopal and F. Wilczek, hep-ph/0011333; D. K. Hong, Acta Phys. Polon. B **32**, 1253 (2001); M. Alford, Ann. Rev. Nucl. Part. Sci. **51**, 131 (2001); T. Schäfer, hep-ph/0304281; D. H. Rischke, Prog. Part. Nucl. Phys. **52**, 197 (2004); H.-c. Ren, hep-ph/0404074.

[18] F. Neumann, M. Buballa and M. Oertel, Nucl. Phys. A **714**, 481 (2003); I. Shovkovy, M. Hanauske and M. Huang, Phys. Rev. D **67**, 103004 (2003); S. Reddy and G. Rupak, nucl-th/0405054.

[19] M. G. Alford, J. A. Bowers and K. Rajagopal, Phys. Rev. D **63**, 074016 (2001); for a review on crystalline color superconductivity see J. A. Bowers, hep-ph/0305301.

[20] P. F. Bedaque and T. Schäfer, Nucl. Phys. A **697**, 802 (2002); D. B. Kaplan and S. Reddy, Phys. Rev. D **65**, 054042 (2002); A. Kryjevski, D. B. Kaplan and T. Schäfer, hep-ph/0404290.

[21] M. Alford and K. Rajagopal, JHEP **0206**, 031 (2002); A. W. Steiner, S. Reddy, and M. Prakash, Phys. Rev. D **66**, 094007 (2002).

[22] J. M. Cornwall, R. Jackiw, and E. Tomboulis, Phys. Rev. D **10**, 2428 (1974). For a review of the CJT formalism see, for example, V. Miransky, *Dynamical Symmetry Breaking in Quantum Field Theories* (World Scientific, Singapore, 1993).

[23] S. B. Rüster and D. H. Rischke, Phys. Rev. D **69**, 045011 (2004).

[24] S. L. Glashow, Nucl. Phys. **22**, 579 (1961); S. Weinberg, Phys. Rev. Lett. **19**, 1264 (1967). A. Salam, in *Elementary Particle Physics*, edited by N. Svartholm (Almqvist and Wiksell, Stockholm, 1968).

[25] G. W. Carter and D. Diakonov, Phys. Rev. D **60**, 016004 (1999); J. Berges and K. Rajagopal, Nucl. Phys. B **538**, 215 (1999); F. Gastineau, R. Nebauer, and J. Aichelin, Phys. Rev. C **65**, 045204 (2002); D. Blaschke, D. Ebert, K. G. Klimenko, M. K. Volkov, and V. L. Yudichev, hep-ph/0403151.

[26] M. Buballa and M. Oertel, Nucl. Phys. A **703**, 770 (2002); M. Huang, P. F. Zhuang, and W. Q. Chao, Phys. Rev. D **65**, 076012 (2002).

[27] For a comprehensive review of the NJL model approach to quark matter at large density see M. Buballa, hep-ph/0402234.

[28] Y. Nambu and G. Jona-Lasinio, Phys. Rev. **122**, 345 (1961); Phys. Rev. **124**, 246 (1961).

[29] T. D. Fugleberg, Phys. Rev. D **67**, 034013 (2003).

[30] J. I. Kapusta, *Finite-temperature field theory*, (University Press, Cambridge, 1989).

[31] K. Rajagopal and F. Wilczek, Phys. Rev. Lett. **86**, 3492 (2001).

[32] K. Iida and G. Baym, Phys. Rev. D **63**, 074018 (2001) [Erratum-ibid. D **66**, 059903 (2002)]; Phys. Rev. D **65**, 014022 (2002); Phys. Rev. D **66**, 014015 (2002); I. Giannakis and H.-c. Ren, Phys. Rev. D **65**, 054017 (2002); Nucl. Phys. B **669**, 462 (2003); D. N. Voskresensky, nucl-th/0312016; T. Matsuura, K. Iida, T. Hatsuda, and G. Baym, Phys. Rev. D **69**, 074012 (2004); I. Giannakis, D. F. Hou, H.-c. Ren, and D. H. Rischke, hep-ph/0406031.
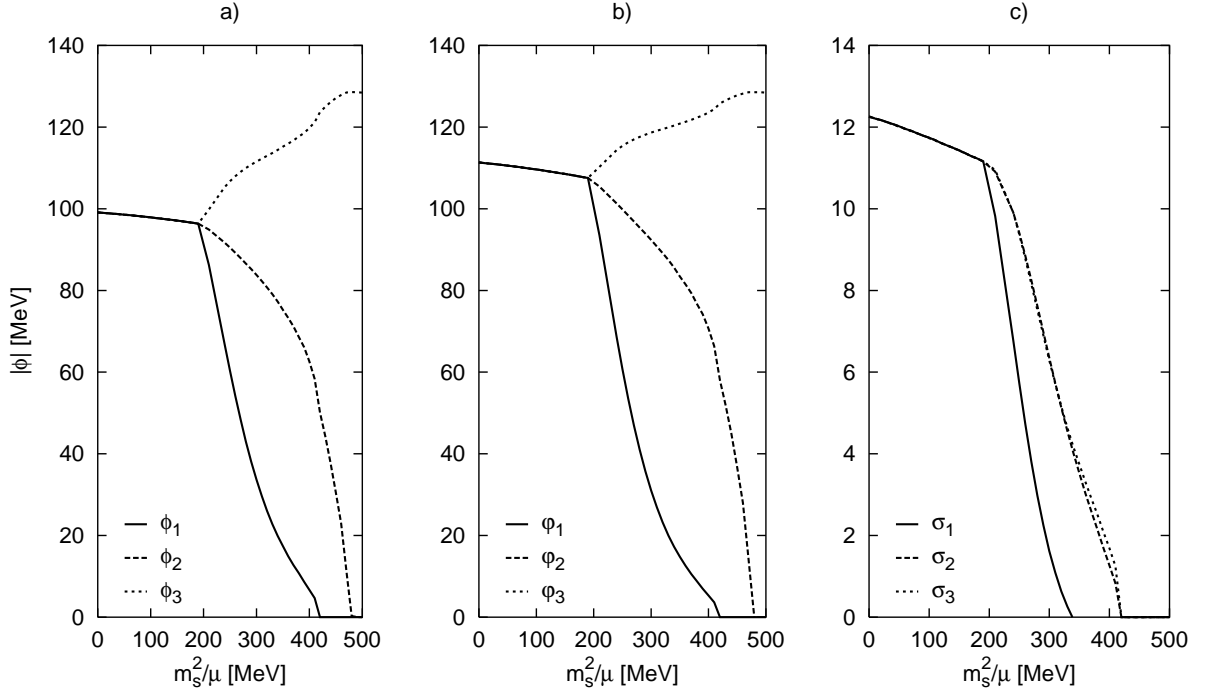
FIG. 2: The absolute values of the gap parameters as a function of m_s^2/μ for neutral color-superconducting quark matter at $T = 0$ and $\mu = 500$ MeV. The actual values of the gap parameters shown in panel a) are negative.
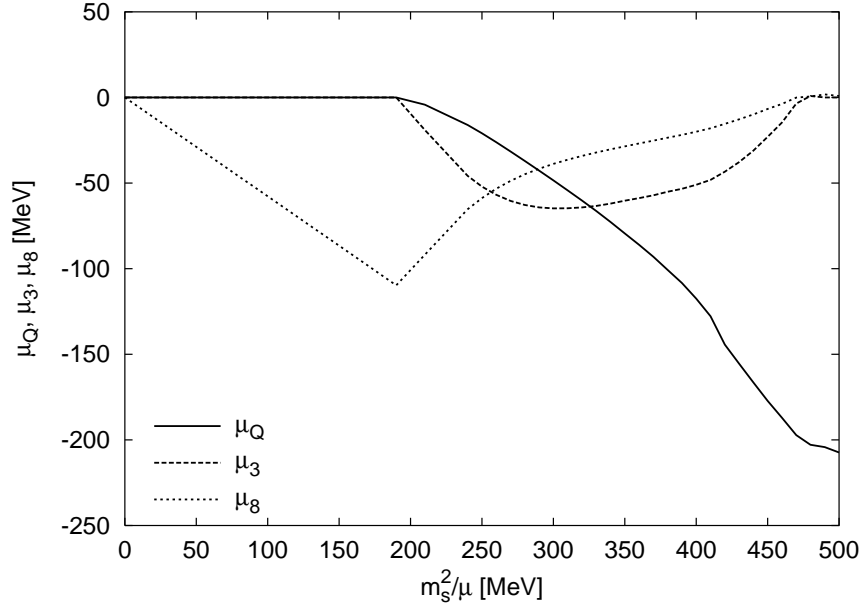

FIG. 3: The electrical and color chemical potentials as a function of m_s^2/μ of electrical and color neutral color-superconducting quark matter at $T = 0$ and $\mu = 500$ MeV.
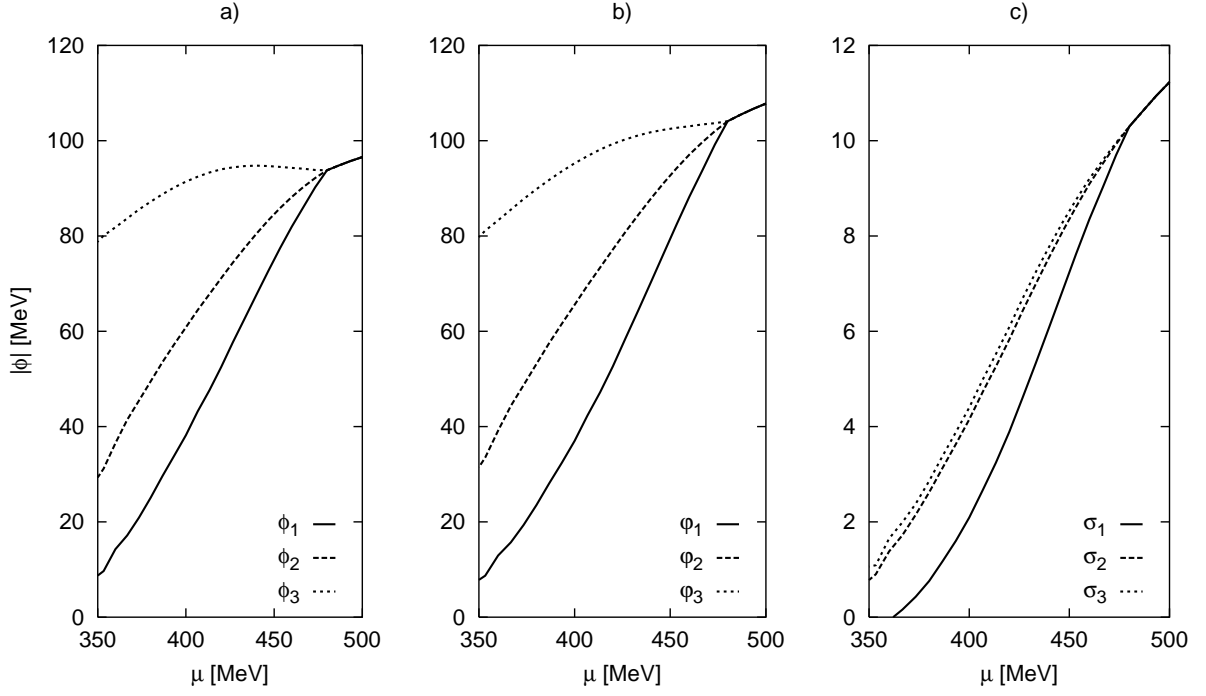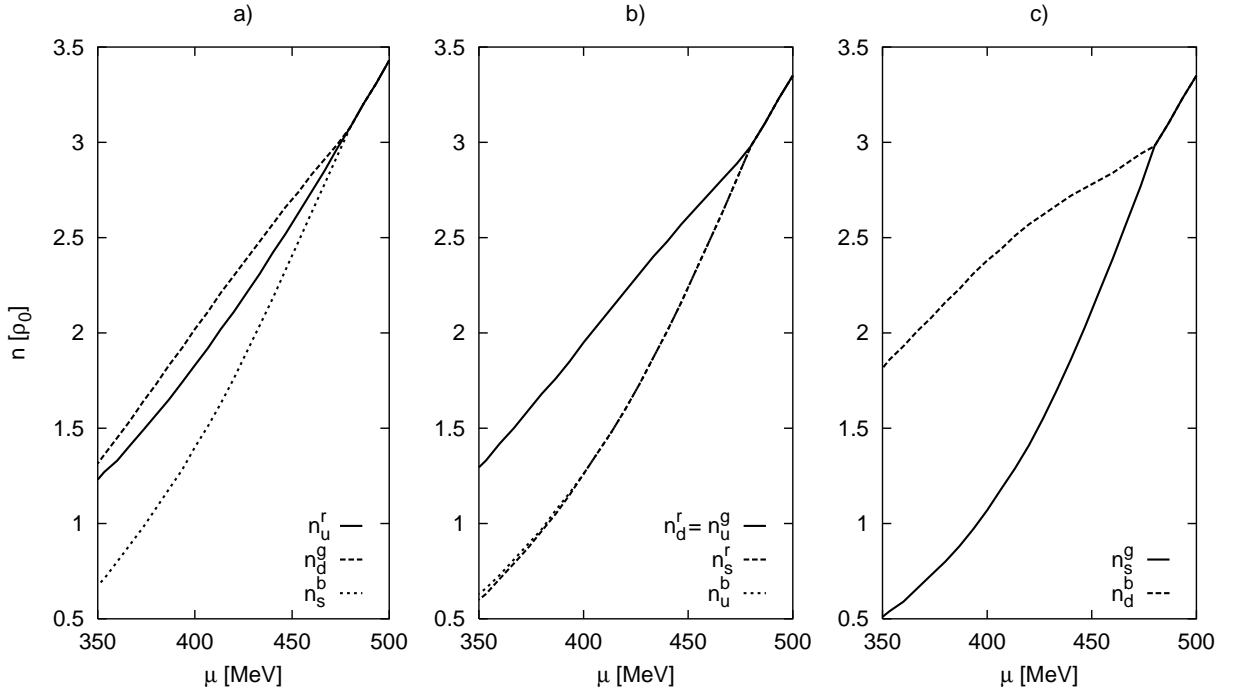
FIG. 4: The absolute values of the gap parameters as a function of μ of electrical and color neutral color-superconducting quark matter at $T = 0$ and $m_s = 300$ MeV. The actual values of the gap parameters shown in panel a) are negative.

FIG. 5: The number densities of each quark color and flavor as a function of μ for electric and color neutral color-superconducting quark matter at $T = 0$ and $m_s = 300$ MeV. The densities are given in units of the saturation density of nuclear matter, $\rho_0 = 0.15$ fm^{-3}.
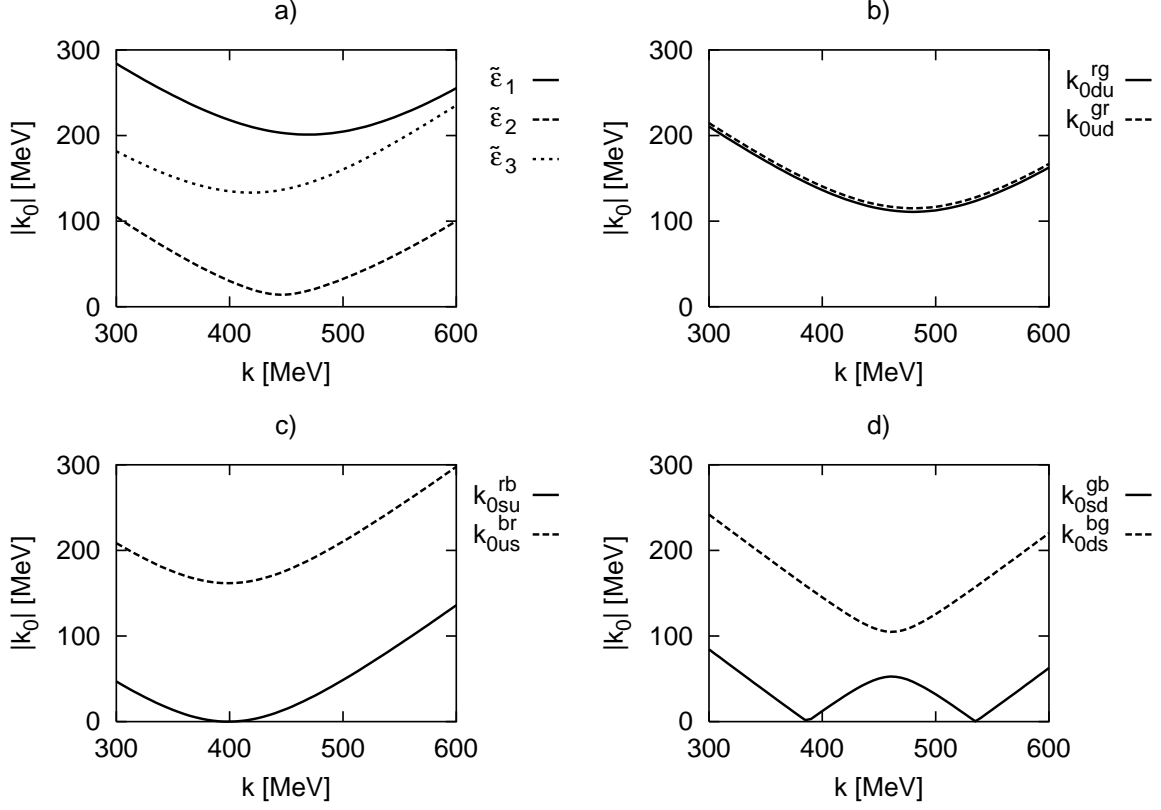
FIG. 6: The quasiparticle dispersion relations for electrical and color neutral color-superconducting quark matter at $T = 0$, $\mu = 500$ MeV, and $m_s = 400$ MeV.
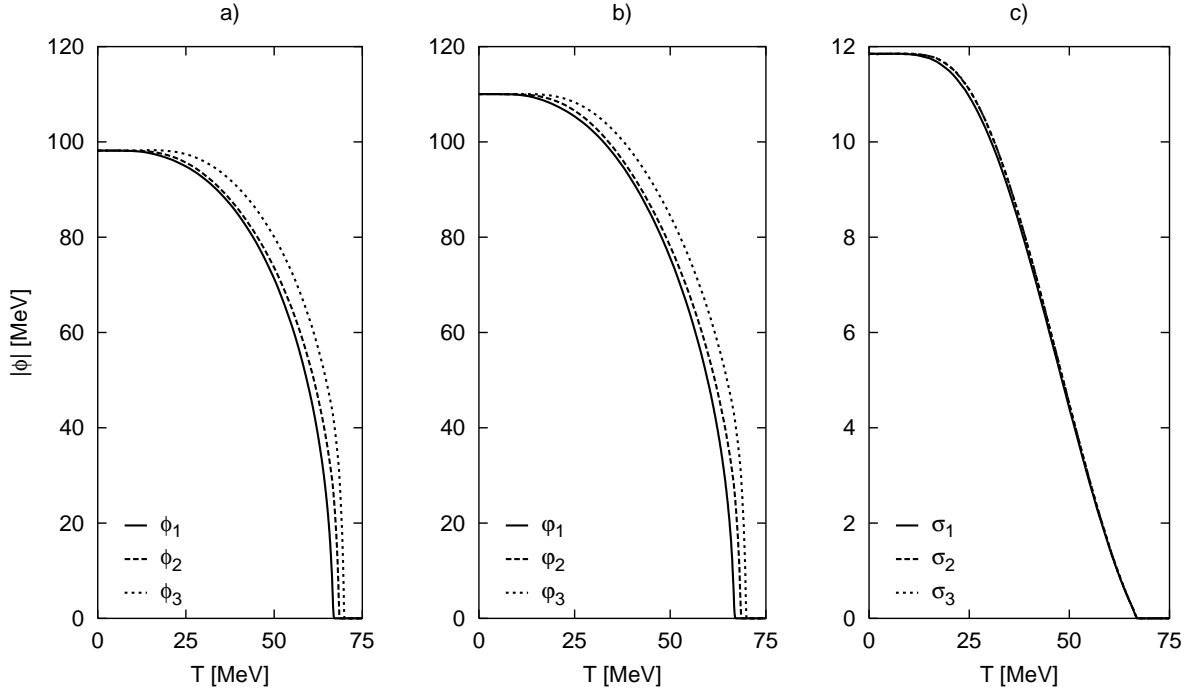
FIG. 7: The temperature dependence of the gaps in the case of a small strange quark mass, $m_s^2/\mu = 80$ MeV. Note that the actual values of the gap parameters shown in panel a) are negative.
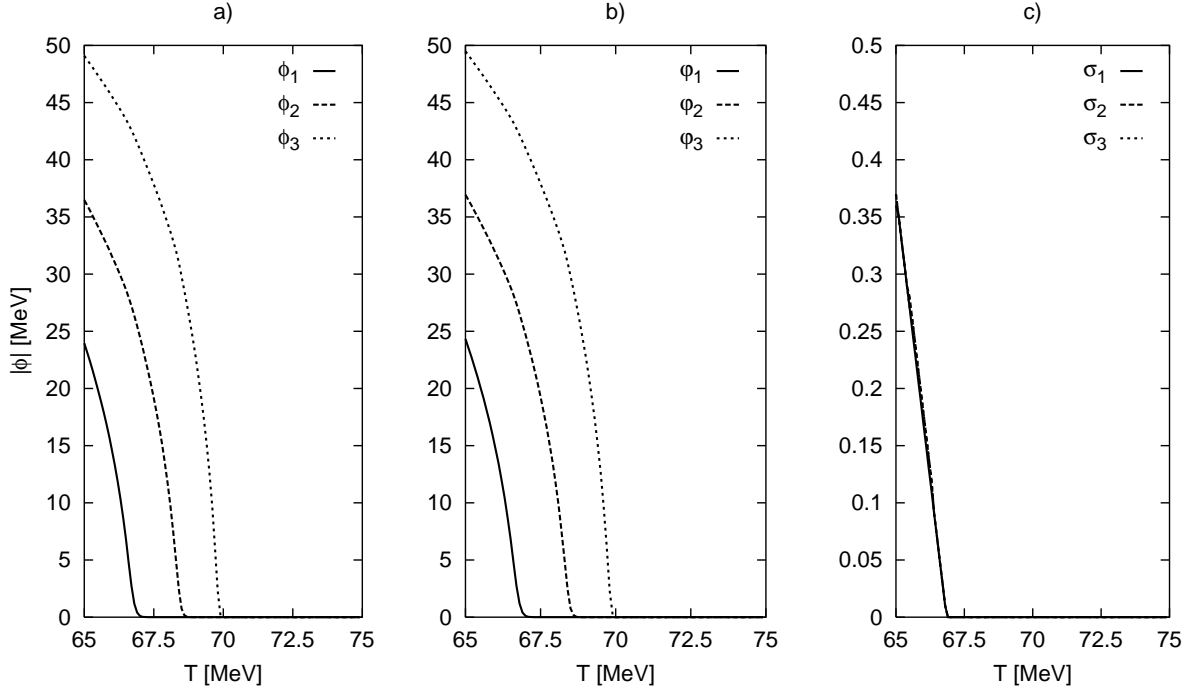
FIG. 8: The near-critical temperature dependence of the gaps in the case of a small strange quark mass, $m_s^2/\mu = 80$ MeV. Note that the actual values of the gap parameters shown in panel a) are negative.
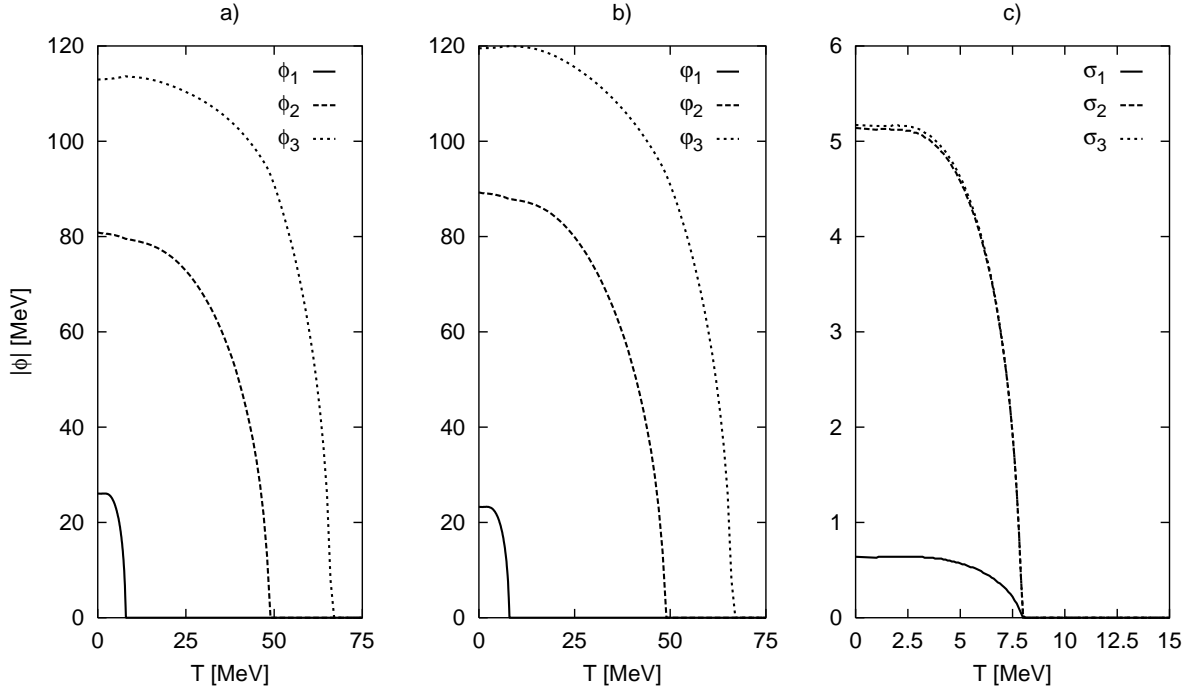

FIG. 9: The temperature dependence of the gaps in the case of a large strange quark mass, $m_s^2/\mu = 320$ MeV. Note that the actual values of the gap parameters shown in panel a) are negative.
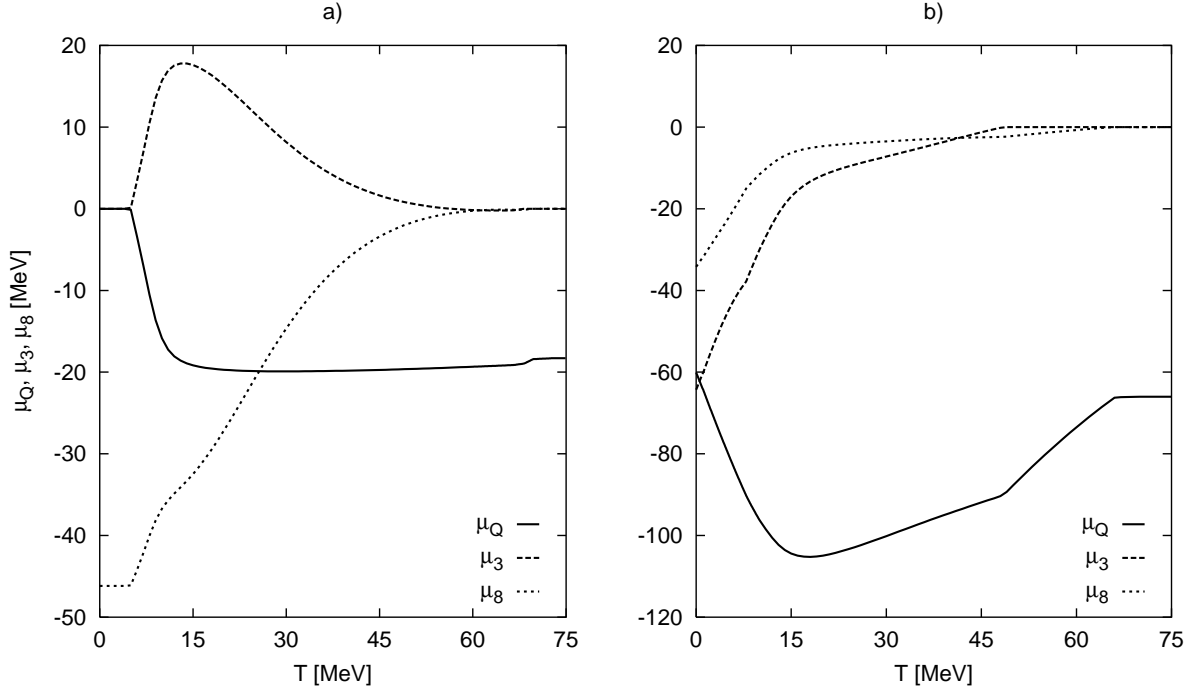
FIG. 10: The temperature dependence of the electrical and color chemical potentials for $m_s^2/\mu = 80$ MeV (left panel) and for $m_s^2/\mu = 320$ MeV (right panel). The quark chemical potential is taken to be $\mu = 500$ MeV.
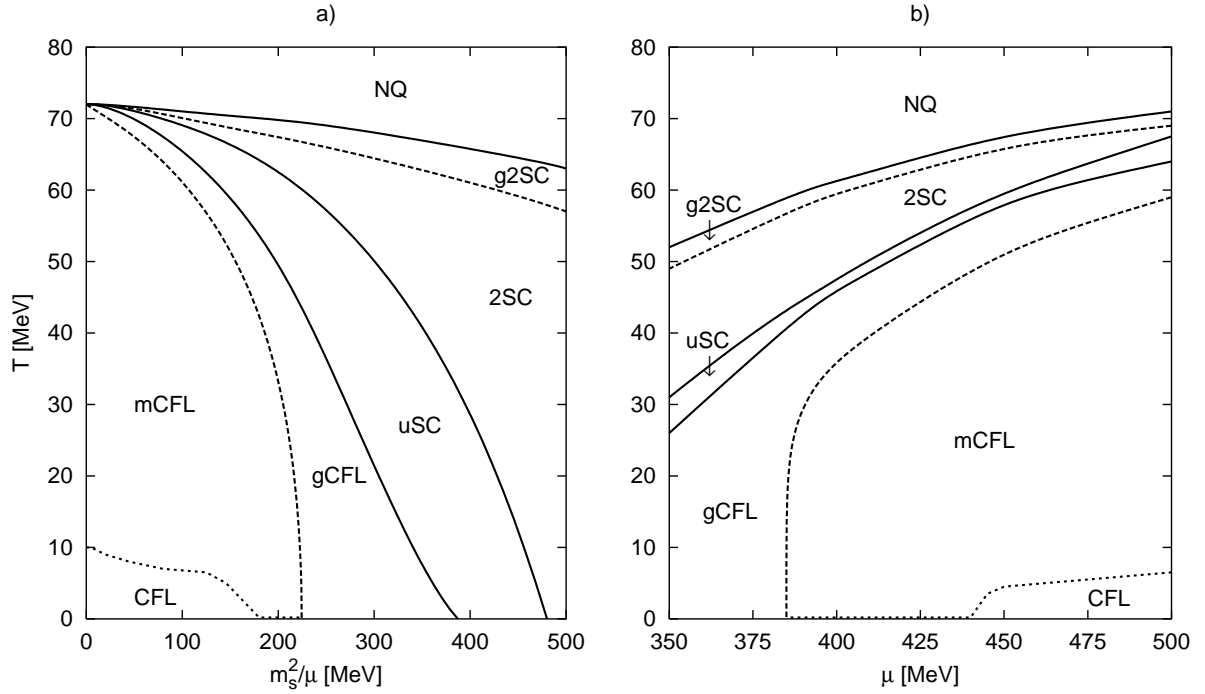

FIG. 11: The phase diagram of neutral three-flavor quark matter in the plane of temperature and m_s^2/μ (left panel) and in the plane of temperature and quark chemical potential (right panel). The results in the left panel are for a fixed value of the quark chemical potential, $\mu = 500$ MeV. The results in the right panel are for a fixed value of the strange quark mass, $m_s = 250$ MeV. The dashed lines are associated with the appearance of additional gapless modes in the spectra. The dotted lines indicate the insulator-metal crossover.